Received December 19, 2020, accepted January 5, 2021, date of publication January 13, 2021, date of current version January 26, 2021.

Digital Object Identifier 10.1109/ACCESS.2021.3051312

Novel Single-Ended-to-Balanced Filter With Reconfigurable Working Modes, Frequency, Bandwidth, and Single/Dual-Band Operations

XIONG CHEN[1], TAO YANG[1], (Senior Member, IEEE), AND PEI-LING CHI[2], (Senior Member, IEEE)

[1]Department of Microwave Engineering, University of Electronic Science and Technology of China, Chengdu 611731, China

[2]Department of Electrical and Computer Engineering, National Chiao Tung University, Hsinchu 300, Taiwan

Corresponding author: Tao Yang (yangtao8314@uestc.edu.cn)

ABSTRACT A novel single-ended-to-balanced (SETB) filtering circuit is proposed in this paper. The proposed circuit not only integrate controllable working modes between SETB filtering and SETB filtering power dividing (FPD) into one unit, but also has multi-level reconfigurable capabilities including tunable center frequencies, bandwidths, and switchable single/dual-band operations. It is constructed by a 5-port symmetrical microstrip network. By properly engineering the transmission response of the even and odd mode of the proposed circuit, the multiple reconfigurable functions can be realized in just one circuit in a mathematically sound way. The working modes between SETB filtering and SETB FPD are switched by leaving the corresponding ports open, while the control of center frequency, bandwidth, and single/dual-band operation is realized by tuning the capacitance value of loaded varactors. Detailed theoretical and experiment results have been given with good agreement.

INDEX TERMS Bandpass filter, dual-band filter, reconfigurable filter, single to balanced filter, single to balanced filtering power divider.

I. INTRODUCTION

Baluns and bandpass filters are essential components in the modern communication system. To reduce system cost and size, balun and filter can be integrated into a single unit to form the so-called single-to-balanced bandpass filter or balun filter, which can transform the single-ended signal to balanced signal while having bandpass characteristics. Various work has been done to develop balun filter [1]–[4]. The desired merit featuring low loss, high selectivity and wide stopband attenuation has been achieved. These designs, however, only afford fixed band applications.

Besides to single-ended-to-balanced bandpass filter, single-ended-to-balanced filtering power-divider (SETB FPD) is another emerging technology. Fig. 1(a) shows the conventional technology that cascades filter, power divider and baluns to obtain split differential outputs. Fig. 1(b) shows the diagram of an integrated SETB FPD that combines the functions of filter, power divider and balun in one single unit. Compared to the conventional cascading solution (Fig. 1(a)), the integrated SETB FPD in Fig. 1(b) will offer a significate size and cost reduction. Fig. 1(c) shows one potential application scenario of the integrated SETB FPD in a differential quadrature downconverter for low-IF or zero-IF receivers [5]–[7]. In this downconverter, the SETB FPD after the low noise amplifier (LNA) integrates the functions of balun, filter and differential power divider, and generates two pairs of differential signals to the mixers, resulting in a compact size and low-cost. To take these advantages, different techniques have been proposed to realize the SETB FPD. A compact, low loss, and planar SETB power divider (PD) was presented in [8] using folded coupled-lines. A planar wideband SETB PD was shown in [9] with high suppression of common-mode (CM) transmission at the center frequency. In [10], a SETB power divider was proposed to implement a 2×4 Bulter Matrix. Antenna beams with very low cross-polarization level were obtained. All these designs have realized single-to-balanced power divider functions with good common-mode rejection. They, however, did not integrate the filter functions. In [11], [12], filter

The associate editor coordinating the review of this manuscript and approving it for publication was Rocco Giofré.

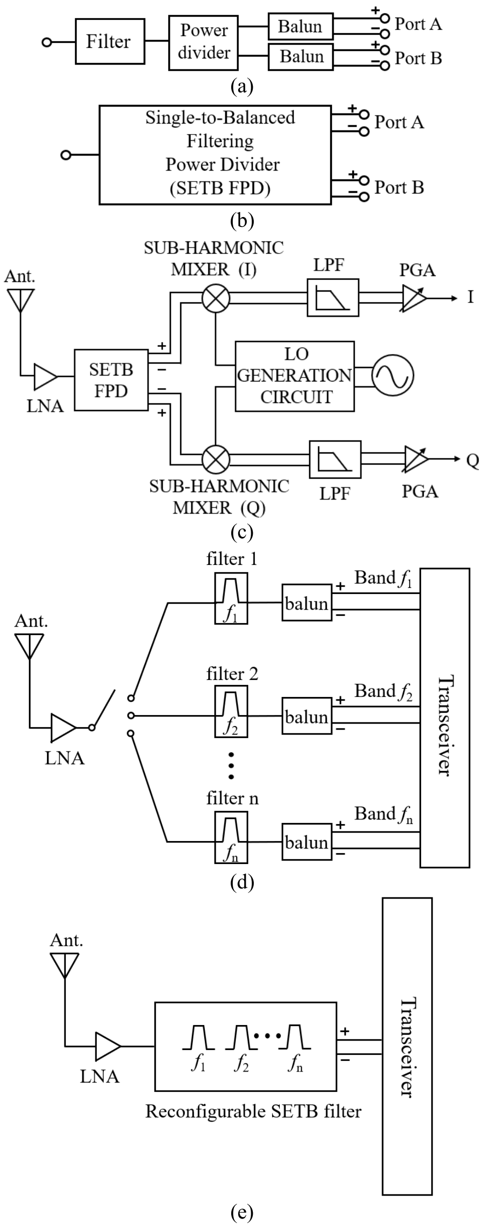

FIGURE 1. (a) Conventional solution of cascading filter, power-divider and balun. (b) Integrated SETB FPD. (c) Typical application of SETB FPD for direct-conversinon receiver. (d) Architecture of a differential multi-band transceiver. (e) Architecture of a reconfigurable differential multi-band transceiver.

functions have been successfully integrated into the SETB PD with good performance. These designs, however, did not have the capability of frequency or passband reconfiguration and cannot afford for multiband applications.

With the development of modern communication technology, Various multi-band filters [13]–[16] are proposed to develop communication systems with multi-band operation mode to increase data capacity. Fig. 1(d) shows a typical architecture for a multi-band differential transceiver with common-mode rejection. In this architecture, the transceiver employs a set of fixed-band filters, baluns, and an antenna switching matrix (ASM) to select the pre-determined (discrete) bands. Due to the requirement of a large number of filters and baluns, the architecture requires a large system size and a high cost. A possible solution to reduce both the size and cost is to employ a reconfigurable SETB filter, as shown in Fig. 1(e). In this case, the ASM was eliminated and the discrete filters and baluns are integrated into one element with frequency agility, significantly reducing the system size and cost. To accomplish the solution, various kinds of reconfigurable single-to-balanced filters are published [17]–[19]. In [17], the functions of single-to-balanced, power dividing, and single-ended filter are achieved within one circuit by changing the capacitive and inductive coupling between the step impedance resonators. In [18], a reconfigurable balun filter was constructed by using stepped impedance resonators; In [19], tunable filtering balun was obtained with constant bandwidth. These works, however, only integrated the filter and baluns. To the authors' best knowledge, no work has been reported to integrate filter, balun, and power divider functions with the capability of frequency and passband reconfiguration for potential multi-band applications such as for multi-band quadrature down/up-converter systems.

In this paper, a novel reconfigurable single-to-balanced filtering circuit is proposed. The design not only integrates controllable working modes between SETB filtering and SETB FPD into one unit, but also has multi-level reconfigurable capabilities including tunable center frequencies and bandwidths, switchable single/dual-band operations. The detailed theoretical equations for the circuit to operate under different modes are given. The reconfigurable functions are achieved by manipulating the coupling coefficient between adjacent resonators and changing the loading conditions of the unused port, i.e. leaving the unused port open-circuited. Microstrip prototype is manufactured and measured, the measured results agree well with the simulation results.

II. STRUCTURE OF THE PROPOSED CIRCUIT

The proposed reconfigurable circuit is shown in Fig. 2. it consists of four open-loop-ring resonators (R_1, R_2, R_3, and R_4) loaded with varactors C_1-C_8 for frequency tuning. Varactors (C_{o1}, C_{o2}, C_{c1} and C_{c2}) are loaded between adjacent resonators and used for the coupling control. Varactors C_{in1}, C_{in2}, C_{out1}, and C_{out2} are used at the input/output port for impedance matching. Note that Port 6 is an open dummy port that can be removed during fabrication. Fig. 3 shows the coupling schematic of the proposed structure. Each resonator consists of an even resonance and an odd resonance. The resonant frequencies of even and odd resonances correspond to the first and second passband, respectively. M_{12}^{o} an M_{12}^{e} represent the odd- and even-mode coupling coefficient between resonator R_1 and R_2, respectively, and M_{34}^{o} and M_{34}^{e} represent the odd- and even-mode coupling coefficient between resonator R_3 and R_4, respectively. By simply manipulating the coupling coefficient between resonators and leaving the unused port open-circuited, the proposed circuit can work in four reconfigurable modes including single-band balun

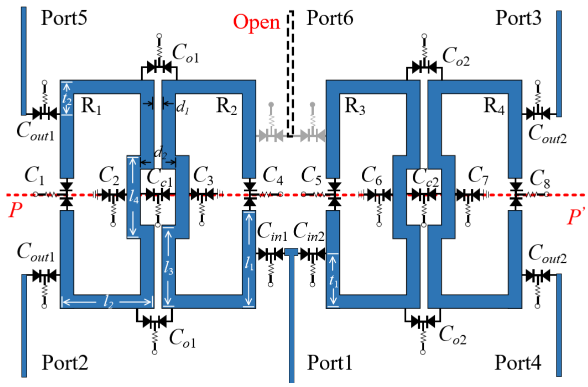

FIGURE 2. Structure of the proposed 6-port symmetric circuit.

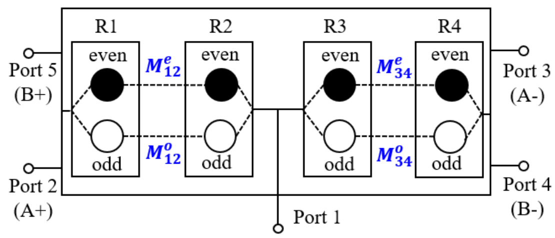

FIGURE 3. Coupling schematic of the proposed structure. The dark node represents the even resonance while the white node represents the odd resonance. The dash line represents the coupling path.

TABLE 1. Coupling and port conditions under different modes.

Working Mode	Coupling Condition	Port Conditions			
		Port2	Port3	Port4	Port5
Dual-band balun filter	$M_{12}^o = M_{34}^o$ $M_{12}^e = -M_{34}^e$	50Ω (B+)	50Ω (B+)	Open	Open
Single-band balun filter	$M_{12}^o = M_{34}^o$ $M_{12}^e = 0$ $M_{34}^e = 0$	50Ω (B+)	50Ω (B+)	Open	Open
Dual-band SETB FPD	$M_{12}^o = M_{34}^o$ $M_{12}^e = -M_{34}^e$	50Ω (A+)	50Ω (A-)	50Ω (B+)	50Ω (B-)
Single-band SETB FPD	$M_{12}^o = M_{34}^o$ $M_{12}^e = 0$ $M_{34}^e = 0$	50Ω (A+)	50Ω (A-)	50Ω (B+)	50Ω (B-)

filtering mode, dual-band balun filtering mode, single band SETB FPD mode, and dual-band SETB FPD mode.

Table 1 summarizes the coupling and port conditions for different working modes. For dual-band balun filter mode, Port 2 and port 3 (or port 4 and port 5) serve as the balun pair (Port A) while Port 4 and port 5 (or port 2 and port 3) are left open. The coupling coefficients are made to be $M_{12}^o = M_{34}^o$, and $M_{12}^e = -M_{34}^e$; To switch the circuit to single-band balun filter mode, the coupling coefficients are made to be $M_{12}^o = M_{34}^o$, and $M_{12}^e = M_{34}^e = 0$. In the SETB FPD modes, Port 2 and 3 are one differential pair while Port 4 and 5 are the other differential pair. Similarly, to make the circuit working

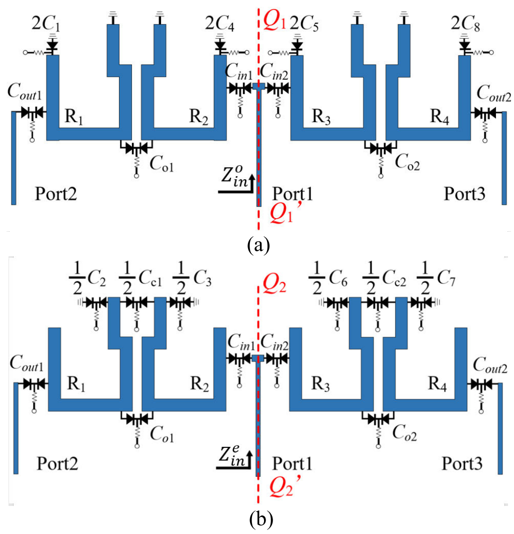

FIGURE 4. (a) Odd-mode half circuit. (b) Even-mode half circuit.

in dual-band SETB FPD mode, the coupling coefficients are made to be $M_{12}^o = M_{34}^o$, and $M_{12}^e = -M_{34}^e$; To switch the circuit to single-band SETB FPD mode, the coupling coefficients are made to be $M_{12}^o = M_{34}^o$, and $M_{12}^e = M_{34}^e = 0$.

Since the proposed structure is symmetric to the *PP*' plane, it can be analyzed using the even-odd mode method. Fig. 4(a) and (b) show the odd-mode and even-mode half circuits of the proposed six-port symmetrical network. Port 1 is the single-ended port for all working modes. The detailed working principle of the proposed circuit will be studied in the following section.

III. WORKING PRINCIPLES OF THE PROPOSED RECONFIGURABLE MULTIFUNCTIONAL FILTER

A. DUAL-BAND BALUN FILTER MODE

To work in dual-band balun filter mode, the odd- and even-mode half circuits need to satisfy the following equation (1), The detailed derivation of equation (1) is given in Appendix A.

For the first passband f_o :

$$\begin{cases} S_{11}^o = 0, S_{21}^o = S_{31}^o = \dfrac{\sqrt{2}}{2} & \text{at } f = f_o \quad (1a) \\ S_{11}^e = -1, S_{21}^e = S_{31}^e = 0 & \text{at } f = f_o \quad (1b) \end{cases}$$

For the second passband f_e :

$$\begin{cases} S_{11}^e = 0, S_{21}^e = -S_{31}^e = \dfrac{\sqrt{2}}{2} & \text{at } f = f_e \quad (1c) \\ S_{11}^o = -1, S_{21}^o = S_{31}^o = 0 & \text{at } f = f_e \quad (1d) \end{cases}$$

where f_o and f_e are the passband frequencies of the odd and even mode half-circuits and are also used as the first and second passband of the dual-band balun filter; S_{ij}^e and S_{ij}^o (i, j = 1, 2, 3) are the *S*-parameters of the even- and odd-mode half-circuits, respectively.

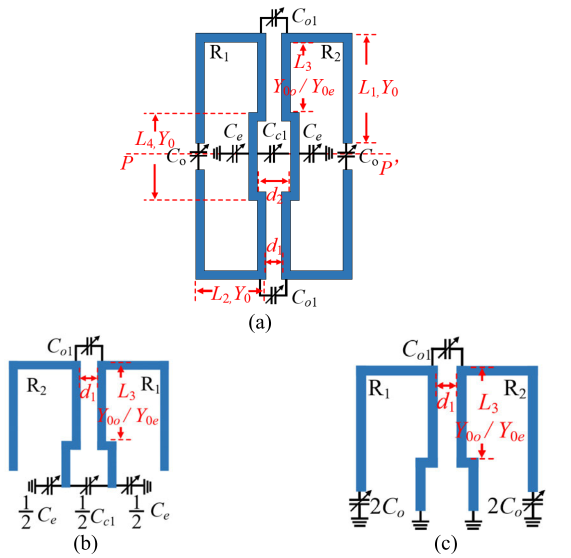

FIGURE 5. **(a) Coupling structure. (b) Even-mode half-circuit of the coupling structure. (c) Odd-mode half-circuit of the coupling structure.**

Equation (1) gives the condition for the proposed circuit to achieve dual-band balun filter function. Equation (1a) implies that the odd-mode half circuit of the corresponding six-port network needs to behave as an equal-phase power-divider, while equation (1c) shows that the even-mode half circuit needs to behave as an out-of-phase power-divider (balun). These two equations can be satisfied by setting the coupling coefficient as $M_{12}^{o} = M_{34}^{o}$ and $M_{12}^{e} = -M_{34}^{e}$. With the requirement of the coupling coefficient being met, signal from port 1 will be equally split to port 2 and 3 in phase for the odd-mode half circuit and out of phase for the even-mode circuit due to the symmetry property.

The capability of the proposed structure to achieve $M_{12}^{o} = M_{34}^{o}$ and $M_{12}^{e} = -M_{34}^{e}$ can be studied using the classic coupled-resonator theory [20]. Fig. 5 shows the coupling structure that is used to extract the coupling coefficients, and the extracted even- and odd-mode coupling coefficients versus the coupling varactors C_{c1} and C_{o1} are shown in Fig. 6. In this paper, the negative coupling value refers to the magnetic coupling while the positive coupling refers to the electric coupling. From Fig. 6(a), the even-mode coupling coefficient M_{12}^{e} can be controlled by tunning C_{c1}. As C_{c1} increases, M_{12}^{e} changes from negative to positive. The physical principle for this transition is that the coupling between the adjacent resonators is dominated by magnetic coupling in nature when the coupling varactors C_{c1} is 0 [20]; as C_{c1} increase from 0, additional electric coupling is introduced, and cancels the magnetic coupling, resulting in decreasing total coupling (magnitude of M_{12}^{e}). When C_{c1} keeps increasing and reaches a transition value (C_T), the electric coupling cancels out the magnetic couplings, zero total coupling is achieved and the passband is eliminated. As C_{c1} increases further and exceed C_T, the electric coupling will dominate, changing the sign of M_{12}^{e} from negative to be positive.

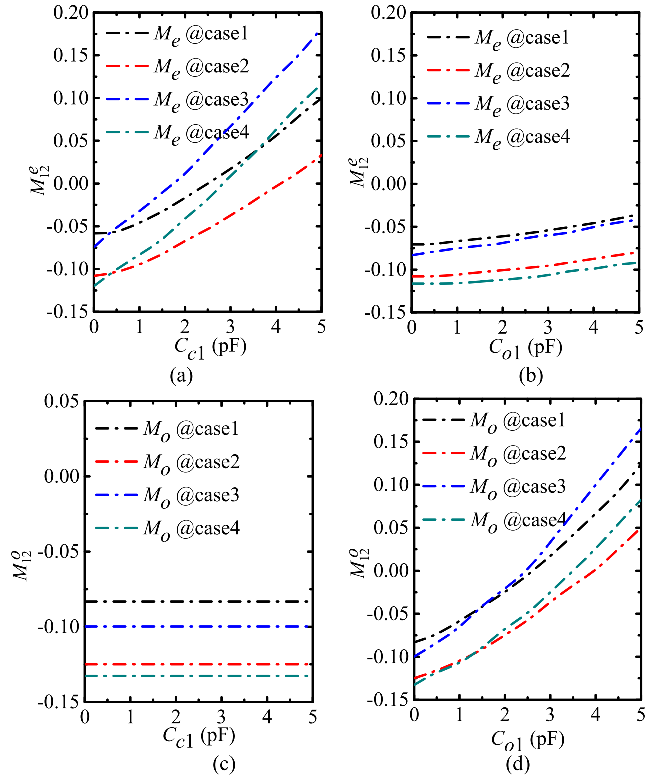

FIGURE 6. **(a) Even-mode coupling coefficient M_{12}^{e} versus C_{c1} while $C_{o1} = 0$ pF. (b) Even-mode coupling coefficient M_{12}^{e} versus C_{o1} while $C_{c1} = 0$ pF. (c) Odd-mode coupling coefficient M_{12}^{o} versus C_{c1} while $C_{o1} = 0$pF. (d) Odd-mode coupling coefficient M_{12}^{o} versus C_{o1} while $C_{c1} = 0$pF. Case1: $L_1 = 12.5$mm, $L_2 = 6$mm, $L_4 = 8$mm, $L_5 = 10$mm, $Y_{0e} = 0.0237$S, $Y_{0o} = 0.0327$S. Case2: $L_1 = 12.5$mm, $L_2 = 6$mm, $L_4 = 8$mm, $L_5 = 10$mm, $Y_{0e} = 0.0222$S, $Y_{0o} = 0.039$S. Case3: $L_1 = 14$mm, $\theta_2 = 6$mm, $L_4 = 9.5$mm, $L_5 = 10$mm, $Y_{0e} = 0.0237$S, $Y_{0o} = 0.0327$S. Case4: $L_1 = 14$mm, $L_2 = 6$mm, $L_4 = 9.5$mm, $L_5 = 10$mm, $Y_{0e} = 0.0222$S, $Y_{0o} = 0.039$S. For all cases, $Y_0 = 0.027$S $f_e = 1.2$GHz, $f_o = 0.6$GHz, $\varepsilon_r = 10.2$ and substrate thickness = 25mils.**

Fig.6 (b) shows M_{12}^{e} versus C_{o1}. It is found that M_{12}^{e} keeps negative, and does not change significantly when C_{o1} increases. This is due to the reason that the tap position of C_{o1} is at the place where electric field distribution in even-mode excitation is relatively weak, and the effective electric coupling introduced by C_{o1} is also weak. Fig. 6(c) and (d) shows the odd-mode coupling coefficients M_{12}^{o} versus C_{c1} and C_{o1}, respectively. Similarly, the M_{12}^{o} does not change with C_{c1}, but changes from negative to positive as C_{o1} increase.

Therefore, it is concluded that M_{12}^{e} can be independently controlled from negative to positive by C_{c1} while not affecting M_{12}^{o}; M_{12}^{o} can be independently controlled from negative to positive by C_{o1} while not affecting M_{12}^{e} much. With the even- and odd- mode coupling coefficient being independently controlled, the bandwidth of the two passband can be controlled separately. the coupling condition ($M_{12}^{o} = M_{34}^{o}$ and $M_{12}^{e} = -M_{34}^{e}$) in Table 1 can be easily realized by controlling the varactors of C_{c1} and C_{o1} to satisfy the condition (1a) and (1c). Fig. 7(a) shows the simulated transmission response of the even- and odd-mode equivalent circuits by appropriately setting C_{c1} and C_{o1} to make $M_{12}^{o} = M_{34}^{o}$ and $M_{12}^{e} = -M_{34}^{e}$.

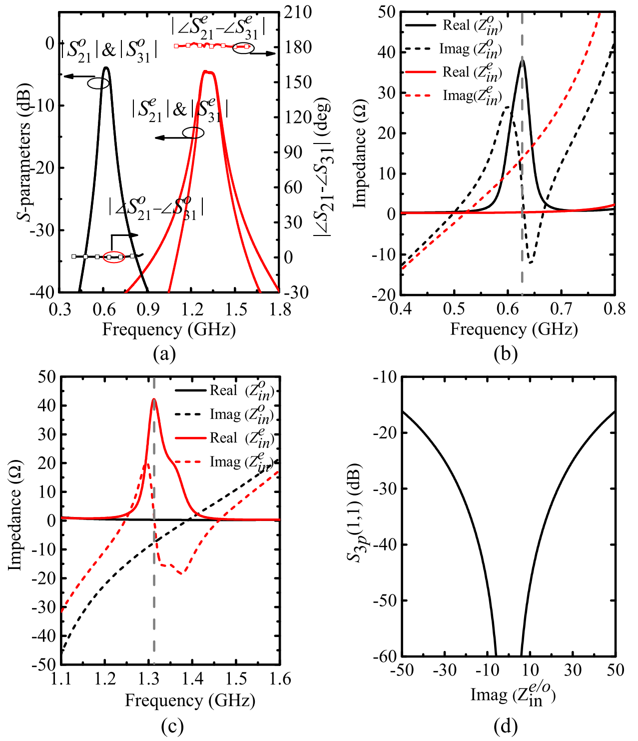

FIGURE 7. (a) Simulated transmission coefficient of the odd- and even-mode half circuit. (b) Simulated input impedance of odd- and even- mode half-circuit at frequency tuning range of first band. (c) Simulated input impedance of odd- and even- mode half-circuit at frequency tuning range of second band. (d) Imaginary part of $S_{3p}(1,1)$ versus $Z_{in}^{e,o}$. All the simulation results are based on circuit dimension given in Table 2 and substrate with thickness = 25mils, $\varepsilon_r = 10.2$.

As can be observed clearly, in-phase equal power dividing is obtained at f_o for odd-mode half circuit and a nice balun filter response has been obtained at f_e for the even-mode half-circuit. Meanwhile, since the even/odd mode resonant frequencies of proposed resonators in Fig. 2 are significantly different from each other, the even-mode half circuit exhibits bandstop response (total reflection) at the first passband f_o, and the odd-mode half circuit exhibits bandstop response (total reflection) at the second passband f_e, satisfying $S_{21}^e = S_{21}^e = 0$ at $f = f_o$ and $S_{21}^o = S_{21}^o = 0$ at $f = f_e$ in (1b) and (1d),respectively.

$S_{11}^e = -1$ at $f = f_o$ and $S_{11}^o = -1$ at $f = f_e$ needs to be satisfied as given in (1b) and (1d) to obtain good impedance matching at the common port (Port 1) under dual-band balun filter mode. Defining Z_{in}^e and Z_{in}^o to be the even and odd mode input impedance of port 1 respectively, it requires that both the real and imaginary part of $Z_{in}^e|_{f=f_o}$ and $Z_{in}^o|_{f=f_e}$ to be zero. However, under most circumstances, the real part of $Z_{in}^e|_{f=f_o}$ and $Z_{in}^o|_{f=f_e}$ can be maintained to be zero but their imaginary part may deviate away from zero as shown in Fig. 7(b) and (c). The sensitivity of $S_{3p}(1,1)$ versus $Imag(Z_{in}^e)|_{f=fo}$ and $Imag(Z_{in}^o)|_{f=fe}$ is studied using equation (8) in appendix A and shown in Fig.7 (d), where S_{3P} is defined to be the S-parameters of the three-port dual-band balun filter. From equation (8) in appendix A, it is found that the nonzero $Imag(Z_{in}^e)|_{f=fo}$ and nonzero $Imag(Z_{in}^o)|_{f=fe}$ will only affect the reflection coefficient $S_{3p}(1,1)$ and not affect the amplitude and phase imbalance between $S_{3P}(2,1)$ and $S_{3P}(3,1)$. From fig.7 (d), $S_{3p}(1,1)$ reaches ideal zero when $Imag(Z_{\text{in}}^e)|_{f=f1}$ and $Imag(Z_{\text{in}}^o)|_{f=f2}$ are zero, and deteriorates when $Imag(Z_{\text{in}}^e)|_{f=f1}$ and $Imag(Z_{\text{in}}^o)|_{f=f2}$ deviate from zero. However, $S_{3p}(1,1)$ can still keep better than an acceptable level of -17 dB, as long as $Imag(Z_{\text{in}}^e)|_{f=f1}$ and $Imag(Z_{\text{in}}^o)|_{f=f2}$ are less than 50Ω. A small value of $Imag(Z_{\text{in}}^e)|_{f=f1}$ and $Imag(Z_{\text{in}}^o)|_{f=f2}$ will make S_{11}^e close to -1 at $f = f_o$ and S_{11}^o close to -1 at $f = f_e$. Thus, conditions (1b) and (1d) can be approximately satisfied.

In summary, with all the conditions from (1a) to (1d) successfully met, a dual-band balun filter is readily obtained. An EM simulation result is given in fig. 8(a) with all the conditions in equation (1) satisfied, as can be seen, the circuit shows dual-band balun filter characteristic.

B. DUAL-BAND SINGLE-ENDED-TO-BALANCED FILTERING POWER DIVIDER

To work in dual-band SETB FPD mode, the odd- and even-mode half circuits need to satisfy the following equation (detailed derivation process is given the Appendix B),

For the first passband f_o :

$$\begin{cases} S_{11}^o = \dfrac{1}{3}, S_{21}^o = S_{31}^o = \dfrac{2}{3} & \text{at } f = f_o \quad (2a) \\ S_{11}^e = -1, S_{21}^e = S_{31}^e = 0 & \text{at } f = f_o \quad (2b) \end{cases}$$

For the second passband f_e:

$$\begin{cases} S_{11}^e = \dfrac{1}{3}, S_{21}^e = -S_{31}^e = \dfrac{2}{3} & \text{at } f = f_e \quad (2c) \\ S_{11}^o = -1, S_{21}^o = S_{31}^o = 0 & \text{at } f = f_e \quad (2d) \end{cases}$$

Equations (2a) and (2c) indicate that the even- and odd-mode half-circuits need to be in-phase and out-of-phase power-dividing, respectively. Besides, the transmission magnitude and reflection magnitude need to be 2/3 and 1/3, respectively. Similar to the dual-band balun filter mode, the in-phase and out-of-phase power-dividing can be realized by setting $M_{12}^o = M_{34}^o$ and $M_{12}^e = -M_{34}^e$. The reflection coefficient of 1/3 for both even- and odd-mode can be realized by adjusting the input coupling capacitance which controlled the input matching at the common input port (Port 1). Meanwhile, equations (2b) and (2d) are met due to frequencies difference between the even and odd resonances, just as discussed for the dual-band balun filter mode. Fig. 8(b) shows the transmission characteristic of the circuit with all the conditions in equation (2) met, nice dual-band single-ended-to-balanced filter power divider is obtained.

C. SINGLE-BAND OPERATION FOR BOTH THE BALUN FILTER AND SINGLE-TO-BALANCED FILTERING POWER DIVIDER

To transform the dual-band operation of the balun filter and the SETB FPD to single-band operation, the coupling coefficients of even-mode frequency, namely M_{12}^e and M_{34}^e, are set

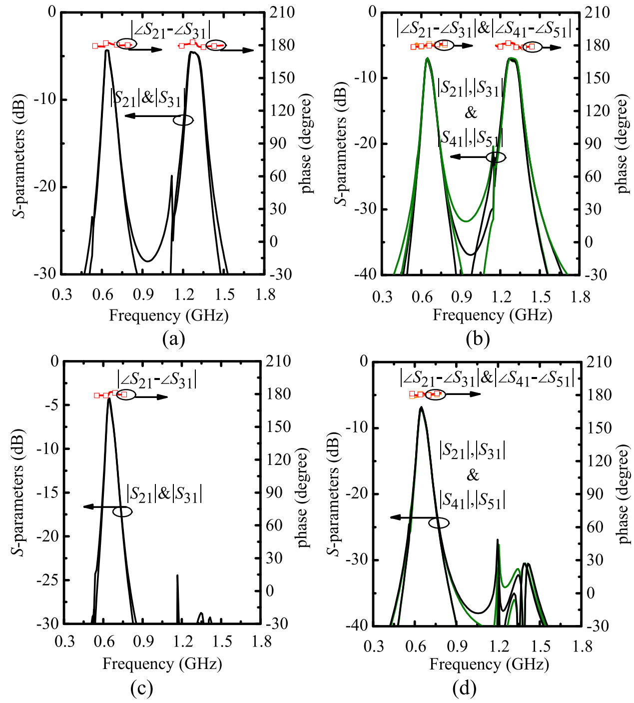

FIGURE 8. Simulated transmission response of the proposed circuit under (a) dual-band balun mode. (b) dual-band SETB FPD mode. (c) single-band balun mode. (d) single-band SETB FPD mode. All the simulation results are based on circuit dimension given in Table 2 and substrate with thickness = 25mils, ε_r = 10.2.

as zero by changing C_{c1} and C_{c2} to the transition value C_T while keeping the odd mode coupling coefficient unchanged. As a consequence, the even-mode passband in both the balun filter and SETB FPD will be eliminated due to zero coupling for even-mode resonances. As shown in Fig. 8(c) and (d), by setting M_{12}^e and M_{34}^e to zero, nice single-band balun filter and SETB FPD response can be obtained.

IV. SIMULATIONS AND MEASUREMENTS

For demonstration purposes, Chebyshev filter prototype is designed for the dual-band balun filter and dual-band single-to-balanced filtering power divider. The initial first and second passbands are chosen to be 0.6 GHz and 1.2 GHz, respectively, and the fractional bandwidths are initially chosen as 5%. The required coupling coefficients and external quality factors can be calculated using the method given in [20].

The proposed circuit with the function of reconfigurable balun filter and single-to-balanced filtering power-divider were fabricated on Rogers 6010(ε_r = 10.2) with thickness h = 25 mils. Varactors MA46H202 (C_1, C_4, C_5, C_8) and MA46H204 (C_2, C_3, C_6, C_7, C_{out1}, C_{out2}) from MACOM are used for frequency tuning; MA46H203(C_{in1}, C_{in2}) are used for adjusting the external quality factor at input/output ports; MA46H204(C_{c1}) and MA46H200(C_{c2}, C_{o1}, C_{o2}, C_{o3}, C_{o4}) are used to control the interstage coupling. Varactors C_{c1} and C_{c2} are placed at the bottom of the circuits through

TABLE 2. Physical dimensions of the fabricated circuits. unit: mm.

l_1	l_2	l_3	l_4	t_1	t_2	d_1	d_2
12.5	8	10	10	8	2	0.6	2.6

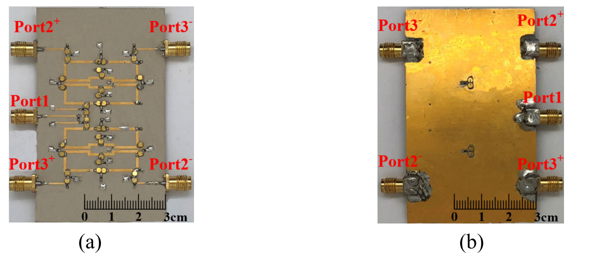

FIGURE 9. Photograph of the fabricated circuits. (a) Top view. (b) Bottom view.

metallic vias. Note that they can be also placed at the top side by increasing d_1. The physical dimensions of the circuits are given in Table 2. The fabricated circuit is shown in Fig. 9.

To work as a dual-band balun filter, port 1 is used as the single-ended input port, port 2 (A+) and port 3 (A-) (or port 4 and port 5) are the balanced output ports while leaving port 4 and port 5 (or port 2 and port 3) open-terminated. Note that the open-terminated condition is achieved by simply leaving the corresponding ports floating.

When working under the dual-band SETB FPD mode, port 1 serves as the single-ended input port, port 2 (A+) and port 3 (A−), port 4 (B+) and port 5 (B−) are the balanced output ports. The dual-band balun filter and dual-band single-to-balanced filtering power-divider were measured using the four-port vector network analyzer Keysight E5071C. As a more intuitive way to describe circuits with balanced ports, mix-mode S-parameters are used instead of single-ended S-parameters. Using the method given in [21], the measured single-ended S-parameters can be transformed into mix-mode S-parameters (See Appendix C).

A. SIMULATED AND MEASURED RESULTS FOR THE DUAL-BAND BALUN FILTER

Fig.10 (a) and (b) show the measured and simulated mix-mode S-parameters of the circuit under dual-band balun filter mode when the first band is tuned and the second band is fixed at 1.3 GHz. The measured results show that the first passband can be tuned from 0.55 GHz to 0.72 GHz, corresponding to a fractional tuning range of 26.8%. The transmission coefficient S_{ds21} with the relative bandwidth (−1dB bandwidth) of about 5% varies from −1.4 dB to −3.3 dB for the tuned first passband and 3.6 dB to 3.7 dB for the fixed second passband. The measured common-mode suppression S_{cs21} is better than −27dB at the passband frequency in all tuning state. The measured S_{ss11} is below −12 dB in the entire tuning range, indicating good impedance match at the input port.

Fig.10 (c) and (d) show the measured and simulated mix-mode S-parameters of the dual-band balun filter when the first passband is fixed at 0.6 GHz. The second passband frequency has a fractional tuning range of 17.9%, covering

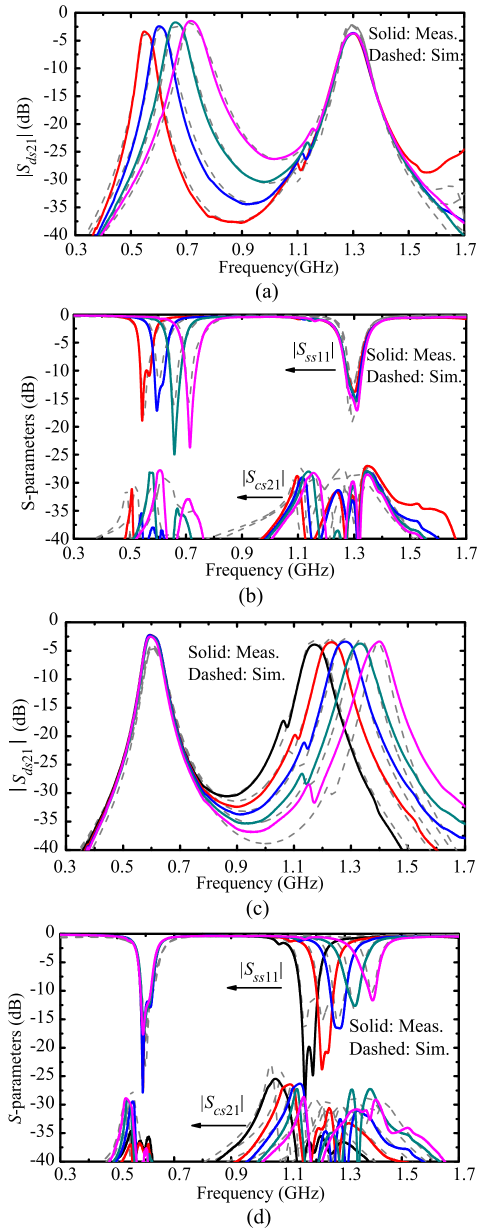

FIGURE 10. **Simulated and measured results of the balun filter in dual-band mode. (a) S_{ds21} for the first-band tuning. (b) S_{ss11} and S_{cs21} for the first-band tuning. (c) S_{ds21} for the second-band tuning. (d) S_{ss11} and S_{cs21} for the second-band tuning.**

from 1.17 GHz to 1.4 GHz. The transmission coefficient S_{ds21} with relative bandwidth (−1 dB bandwidth) of about 5% vary from −3.5 dB to −3.9 dB for the tuned second passband and −2.2 dB to −2.5 dB for the fixed first passband. As shown in Fig. 10(d), the measured common mode suppression S_{sc21} is better than −27 dB at the passband frequency in all tuning state.

In addition to the independent frequency controlling for the two passbands, the proposed dual-band balun filter can be converted to a single band balun filter by tuning the coupling capacitor C_{c1} and C_{c2} and adjust the even mode coupling coefficient M_{12}^{e} and M_{34}^{e} to be zero. The simulated and measured single-band results are shown in Fig. 11. The first band can be tuned from 0.55 GHz to 0.72 GHz, corresponding to a fractional tuning range of 26.8%. The transmission coefficient S_{ds21} with relative bandwidth (−1 dB bandwidth) of about 5% vary from −1.5 dB to −2.4 dB for all tuning states. The measured common mode suppression S_{sc21} is better than −32 dB at the passband frequency in all tuning state. The suppression at the second band is more than 25 dB.

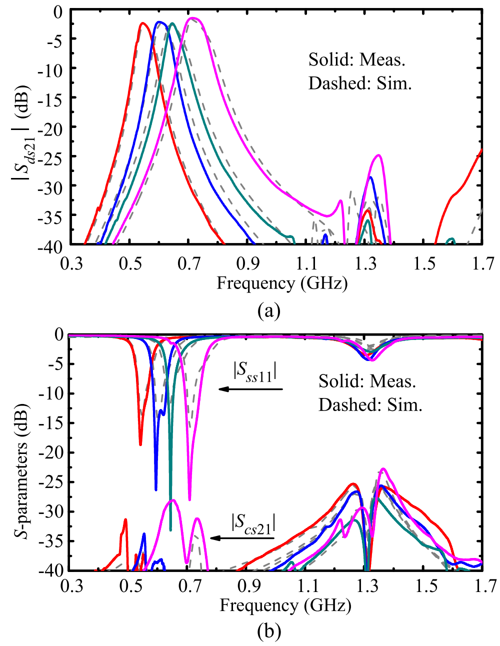

FIGURE 11. **Simulated and measured results of the proposed balun filter in single-band mode (a) S_{ds21}. (b) S_{ss11} and S_{cs21}.**

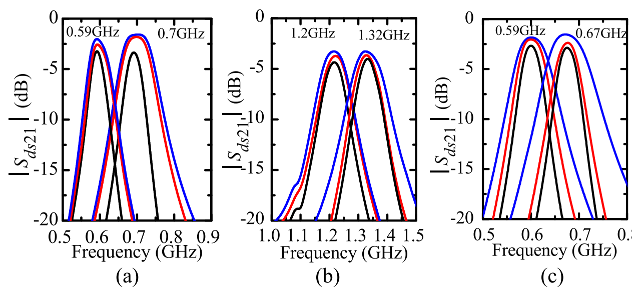

FIGURE 12. **Bandwidth control of the tunable balun filter. (a) Measured S_{ds21} of the first band at 0.59GHz and 0.7GHz. (b) Measured S_{ds21} of the second band at 1.2GHz and 1.32GHz. (c) Measured S_{ds21} at 0.59GHz and 0.7GHz in single-band mode.**

Fig.12 presents the measured results of bandwidth control for the balun filter. Within the entire frequency tuning range, the −1-dB bandwidth can vary from about 30 MHz to 70 MHz for the first band and 40 MHz to 70 MHz for the second band.

B. SIMULATED AND MEASURED RESULTS FOR THE SINGLE-TO-BALANCED FILTERING POWER DIVIDER

Fig.13 (a) and (b) show the measured and simulated mix-mode S-parameters of the dual-band SETB FPD when the second passband is fixed at 1.3 GHz. The first band can be

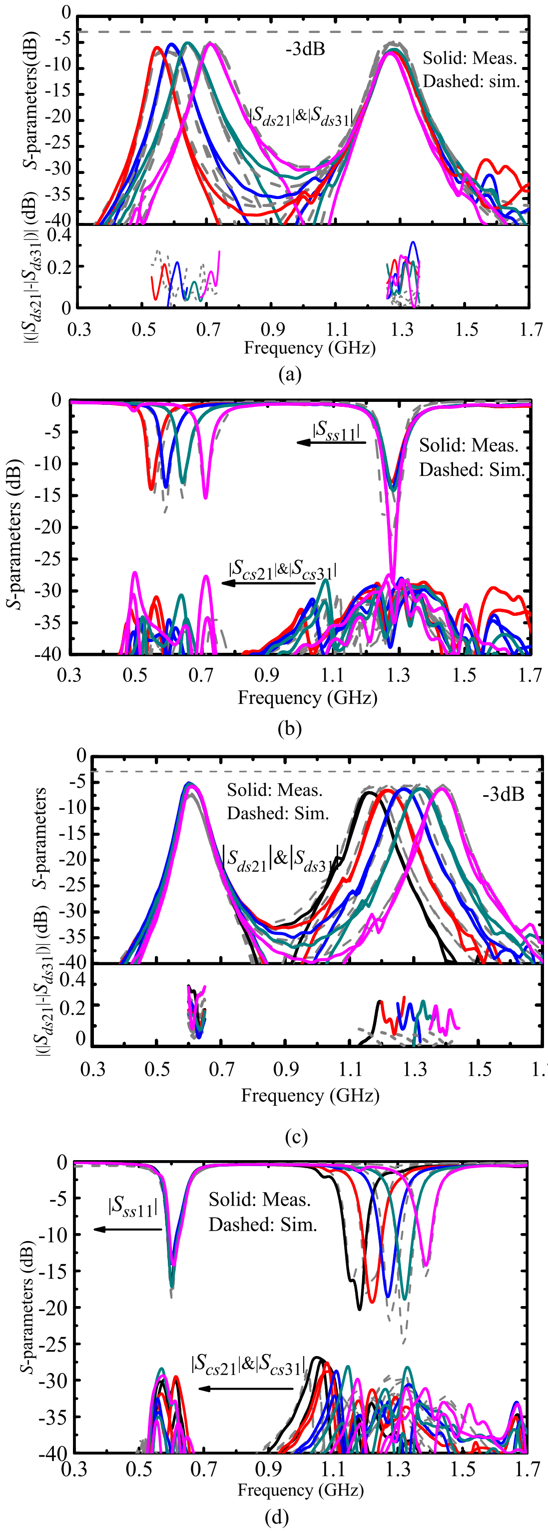

FIGURE 13. **Simulated and measured results of the single-to-balanced filtering power divider in dual-band mode. (a) S_{ds21} and S_{ds31} for first band tuning. (b) S_{ss11}, S_{cs21} and S_{cs31} for first band tuning. (c) S_{ds21} and S_{ds31} for second band tuning. (d) S_{ss11}, S_{cs21} and S_{cs32} for second band tuning.**

tuned from 0.55GHz to 0.7GHz, corresponding to a fractional tuning range of 26.8%. The −1dB relative bandwidth of both the two passbands is about 5%. The measured insertion loss of the first band varies from (2.1+3) dB to (3+3) dB while the insertion loss of the second band changes from (3.4+3) dB to (4+3) dB, where the 3dB comes from the power dividing loss of the output ports. The measured common mode suppression (S_{cs21} and S_{cs31}) is better than 26dB within the entire tuning range. The amplitude imbalance between S_{ds21} and S_{ds31} is less than 0.4dB in all tuning states.

Fig.13 (c) and (d) shows the measured and simulated mix-mode S-parameters of the dual-band single-to-balanced filtering power-divider when the first passband is fixed at 0.6 GHz. For the second band, the passband frequency can be tuned from 1.17 GHz to 1.4 GHz, corresponding to a fractional tuning range of 17.9%. The measured insertion loss of the first band and second band varies from (2.1 + 3) dB to (3+3) dB and (3+3) dB to (4+3) dB, respectively. The measured common mode suppression (S_{cs21} and S_{cs31}) is better than 28dB at the center frequency of all the tuning state. The amplitude imbalance between S_{ds21} and S_{ds31} is again less than 0.4dB in all passbands. Similarly, the second passband of the dual-band SETB FPD can be eliminated, and thus converting the proposed dual-band SETB FPD to a single-band SETB FPD. Fig.14 shows the simulated and measured results for the single-band state, the passband frequency can be tuned from 0.55 GHz to 0.7 GHz with −1dB relative bandwidth about 5% and insertion loss from (2.3 + 3) dB to (3 + 3) dB. The measured common-mode suppression is better than 30dB within the whole tuning range. Fig.15 presents the measured results of bandwidth control for the single to balanced filtering power divider. Within the entire frequency tuning range, the 1-dB bandwidth can vary from about 16 MHz to 40 MHz for the first band and 20 MHz to 50 MHz for the second band.

C. NONLINEARITY MEASUREMENT

The measured input P_{1dB} of the proposed circuit in the dual-band balun filter mode at 0.5GHz, 0.6GHz and 0.7GHz and dual-band SETB FPD mode at 1.2GHz, 1.3GHz, and 1.4GHz are given in fig.16. it shows that the proposed filter can handle power up to around 15.4-23.6dBm in the dual-band balun filter mode and around 13.2-22.6dBm in the dual-band SETB FPD mode. The linearity behavior is similar to other reported work [17], [22], [23] which also use varactors for reconfiguration.

D. COMPARISON WITH OTHER WORKS

Table 3 provides a comparison between related previous work and this work. As can be seen, the proposed circuit is the only one that realized multiple reconfigurable functionalities including dual/single-band balun filter and dual/single-band single-to-balanced filtering power divider. Moreover, the two output passbands can be independently tuned in terms of center frequency and bandwidth, showing a high degree of flexibility and realizing a further cost and volume reduction for the RF communication systems. To the best knowledge of the authors, the proposed circuit is the first implementation of reconfigurable dual-band balun filter and dual-band single-to-balanced filtering power divider. The insertion loss

TABLE 3. Comparison with other works.

Ref.	Filter function		Freq. Tuning (GHz)	1-dB *BW* Tuning (MHz)	3-dB *FBW*	IL(dB)	size ($\lambda_g \times \lambda_g$)	Single to common mode suppression
[13]	Single-band balun filter		1.5~1.9	×	10%-13%	3.2-3.7	0.19×0.61	-
[20]	Dual-band balun filter		Fixed (2.28/2.72)	×	5.3%/ 4.4%	0.9/1	0.46×0.63	-
[21]	Single-band balun filter		Fixed (2GHz)	×	80%	0.9	0.2×0.5	-
[10]	Single-band STB FPD		Fixed (5.9GHz)	×	27%	(3+0.4)	0.77×0.69	<-30 dB (0.3f_0-2.4f_0)
[9]	Single-band SETB FPD	Design 1	Fixed (1.03GHz)	×	≈42%	N/A	0.16×0.4	<-15dB (0-1.55f_0)
		Design 2	Fixed (1.01GHz)	×	≈45%	N/A	0.45×0.2	<-15dB (0-2f_0)
This work	Multi-functions	Dual-band balun filter	0.55-0.72/ 1.17-1.4	30-70/ 40-70	6.77%-10.16%/ 5.91%-8.33%	1.4-3.3/ 3.5-3.9	0.17×0.27	<-26dB (0.6f_0-3.4f_0)
		Single-band balun filter	0.55-0.72	30-70	7.1%-12.3%	1.5-2.4		<-23dB (0.6f_0-3.4f_0)
		Dual-band SETB FPD	0.55-0.72/ 1.17-1.4	16-40/ 20-50	4.6%-10.8%/ 4.7%-7.1%	(2.1+3)-(3+3)/ (3+3)-(4+3)		<-25dB (0.6f_0-3.4f_0)
		Single-band SETB FPD	0.55-0.72	16-40	4.6%-10.8%	(2.3+3)-(3+3)		<-25dB (0.6f_0-3.4f_0)

Note: SETB FPD stands for single-to-balanced filtering power divider; λ_g is the guided wavelength at the lowest frequency of the tuning range; f_0 is lowest frequency in the tuning range; *BW* is the bandwidth; *FBW* is the fractional bandwidth.

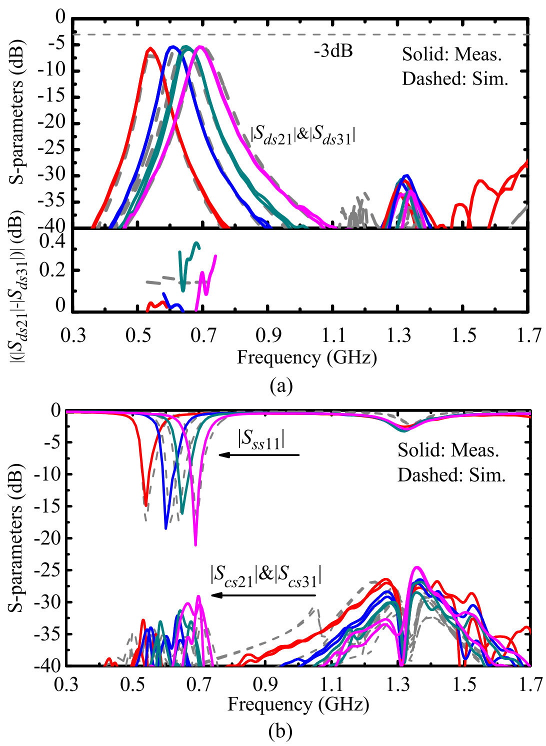

FIGURE 14. Simulated and measured results of the single-to-balanced filtering power divider in single-band mode. (a) S_{ss11} and S_{ds31} for first band tuning, (b) S_{ss11}, S_{cs21} and S_{cs31} for first band tuning.

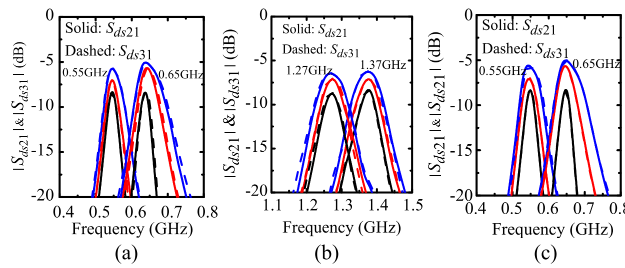

FIGURE 15. Bandwidth control of the STB FPD. (a) Measured S_{ds21} and S_{ds31} of the first band at 0.55GHz and 0.65GHz. (b) Measured S_{ds21} and S_{ds31} of the second band at 1.27GHz and 1.37GHz. (c) Measured S_{ds21} and S_{ds31} at 0.55GHz and 0.65GHz in single-band mode.

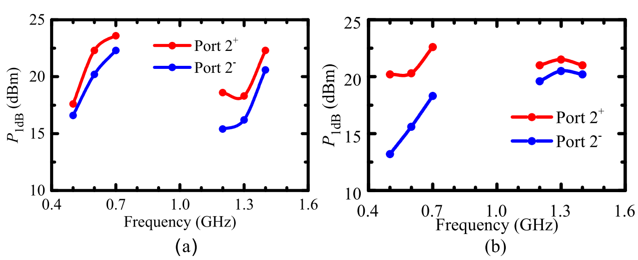

FIGURE 16. (a) Measured P_{1dB} for the dual-band balun mode. (b) Measured P_{1dB} for the dual-band SETB FPD mode.

of the proposed work in dual-band mode is worse than the ones given in [24] and [25], this is due to the reason that the works in [24] and [25] were for fixed-band application and did not offer frequency/bandwidth tuning. The relatively high insertion in the proposed work is due to the low varactor Q, however, the insertion loss of 1.5 to 2.4 dB for the proposed work in single-band balun filter mode is still much smaller than the ones given in [19] with frequency tuning capability, and can be further improved by using RF MEMs varactors [26].

V. CONCLUSION

In this paper, a novel method is proposed to design a multi-functional single-ended to balanced filter. Analytical conditions are extracted to synthesis the multi-functional filter. By properly designing the even and odd mode half-circuit response of a six-port symmetrical circuit, the multi-functions of dual/single-band balun filter and dual/single-band single-ended to balanced filtering power can be integrated into one circuit. Proof-of-concept microstrip prototype is fabricated and measured. Good agreement between simulation and measurement has been achieved. The proposed circuit has advantages in terms of reconfigurable multi-function operation mode and more compact size, dual-band output with independently tunable passband frequency and bandwidth compared with previously published works. With all these distinctive features, the developed prototype can serve as a good candidate in wideband communication systems where multiband balun filter and single-to-balanced filtering power divider are needed.

APPENDIX

A. THEORETICAL DERIVATION OF DUAL-BAND BALUN FILTER

The working principle of the proposed circuit can be analyzed with the help of a conceptual 6-port network shown in Fig.17. Assuming the network is symmetrical along plane PP', it can be analyzed using even- and odd-mode excitations. The three-port even-mode S-parameter S_e and odd-mode S-parameter S_o can be written as

$$S_e = \begin{bmatrix} S_{11}^e & S_{12}^e & S_{13}^e \\ S_{21}^e & S_{22}^e & S_{23}^e \\ S_{31}^e & S_{32}^e & S_{33}^e \end{bmatrix} \tag{3a}$$

$$S_o = \begin{bmatrix} S_{11}^o & S_{12}^o & S_{13}^o \\ S_{21}^o & S_{22}^o & S_{23}^o \\ S_{31}^o & S_{32}^o & S_{33}^o \end{bmatrix} \tag{3b}$$

then the S-parameters of the 6-port network S_{six} can be expressed in terms of S_e and S_o as:

$$S_{six} = \frac{1}{2}\begin{bmatrix} S_e + S_o & S_e - S_o \\ S_e - S_o & S_e + S_o \end{bmatrix} \tag{4}$$

Following the definition of scattering parameters, the S-parameters of the 6-port network can also be expressed as

$$\begin{bmatrix} b_1 \\ b_2 \\ b_3 \\ b_4 \\ b_5 \\ b_6 \end{bmatrix} = S_{six}\begin{bmatrix} a_1 \\ a_2 \\ a_3 \\ a_4 \\ a_5 \\ a_6 \end{bmatrix} = \begin{bmatrix} S_{11} & S_{12} & S_{13} & S_{14} & S_{15} & S_{16} \\ S_{21} & S_{22} & S_{23} & S_{24} & S_{25} & S_{26} \\ S_{31} & S_{32} & S_{33} & S_{34} & S_{35} & S_{36} \\ S_{41} & S_{42} & S_{43} & S_{44} & S_{45} & S_{46} \\ S_{51} & S_{52} & S_{53} & S_{54} & S_{55} & S_{56} \\ S_{61} & S_{62} & S_{63} & S_{64} & S_{65} & S_{66} \end{bmatrix}\begin{bmatrix} a_1 \\ a_2 \\ a_3 \\ a_4 \\ a_5 \\ a_6 \end{bmatrix} \tag{5}$$

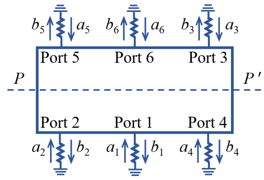

FIGURE 17. Conceptual symmetrical 6-port circuit.

where a_i and b_i are the incident and reflected wave at the port i, respectively.

In dual-band balun filter mode, port 4, port 5 and port 6 are open-circuited, (5) can be written as

$$\begin{bmatrix} B_1 \\ B_2 \end{bmatrix} = S_{six}\begin{bmatrix} A_1 \\ A_2 \end{bmatrix} = \left[\begin{array}{c|c} P_{11} & P_{12} \\ \hline P_{21} & P_{22} \end{array}\right]\begin{bmatrix} A_1 \\ A_2 \end{bmatrix} \tag{6}$$

where $B_1 = [b_1, b_2, b_3]^T$ and $A_1 = [a_1, a_2, a_3]^T$ are 3×1 matrix; $B_2 = [b_4, b_5, b_6]^T$ and $A_2 = [a_4, a_5, a_6]^T$ are 3×1 matrix; P_{11}, P_{12}, P_{21}, and P_{22} are the corresponding sub-matrix of (5) and all have dimensions of 3×3. As port 4, port 5 and port 6 are open-circuited, they have boundary condition as,

$$\begin{aligned} b_4 &= a_4 \\ b_5 &= a_5 \\ b_6 &= a_6 \end{aligned} \tag{7}$$

Combined (7) with (6) the scattering parameters S3p of the reduced three-port circuit can be obtained as,

$$S_{3p} = \left[P_{11} + P_{12}(I - P_{22})^{-1}P_{21}\right] \tag{8}$$

where I is 3×3 unity matrix. To make the reduced three-port circuit behave as a dual-band balun filter, the following equations need to be satisfied in the two passbands,

$$S_{3p}(1,1)|_{f=f_o,\,f_e} = 0 \tag{9a}$$

$$S_{3p}(2,1) = -S_{3p}(3,1)|_{f=f_o,\,f_e} \tag{9b}$$

where f_o and f_e are the passband frequencies of the odd and even mode half-circuit of the circuit in Fig. 2, which are also used as the first and second passband of the dual-band balun filter. To satisfy (9), one possible and practical solution has been found by combining (4), (8) and (9) as,

For the first passband fo:

$$\begin{cases} S_{11}^o = 0, S_{21}^o = S_{31}^o = \dfrac{\sqrt{2}}{2} & \text{at } f = f_o \quad (10a) \\ S_{11}^e = -1, S_{21}^e = S_{31}^e = 0 & \text{at } f = f_o \quad (10b) \end{cases}$$

For the second passband fe:

$$\begin{cases} S_{11}^e = 0, S_{21}^e = -S_{31}^e = \dfrac{\sqrt{2}}{2} & \text{at } f = f_e \quad (10c) \\ S_{11}^o = -1, S_{21}^o = S_{31}^o = 0 & \text{at } f = f_e \quad (10d) \end{cases}$$

It should be noted that the conditions in (10) can be easily validated by put (10) into (4) and the desired balun performance in (9) can be obtained.

B. THEORETICAL DERIVATION OF DUAL-BAND SINGLE-TO-BALANCED FILTERING POWER DIVIDER

When Port 6 in Fig. 17 is imposed with open-circuit condition, it has boundary condition as,

$$b_6 = a_6 \tag{11}$$

The reduced five-port S-parameters S5p can be calculated by combining (11) with (5) as:

$$S_{5p} = \left[P_{11} + P_{12}(I - P_{22})^{-1}P_{21}\right] \tag{12}$$

where I is 1 × 1 unity matrix and P_{11}, P_{12}, P_{21}, P_{22} are the partitioned submatrices of the S_{six}, with dimensions of 5 × 5, 5 × 1, 1 × 5, 1 × 1 respectively. Note that Port 1 here is the single-ended port; Port 2 and 3 are one differential pair while Port 4 and 5 are the other differential pair. For an ideal dual-band SETB FPD, it has,

$$S_{5p}(1,1)|_{f=f_o,f_e} = 0 \tag{13a}$$

$$S_{5p}(2,1) = -S_{5p}(3,1)|_{f=f_o,f_e} \tag{13b}$$

$$S_{5p}(4,1) = -S_{5p}(5,1)|_{f=f_o,f_e} \tag{13c}$$

$$\left|S_{5p}(2,1)\right| = \left|S_{5p}(4,1)\right|_{f=f_o,f_e} \tag{13d}$$

To satisfy (13), one feasible set of condition has been found by combining (4) (12) and (13) as,

For the first passband fo:

$$\begin{cases} S_{11}^e = -1, S_{21}^e = S_{31}^e = 0 & \text{at } f = f_o \quad (14a) \\ S_{11}^o = \frac{1}{3}, S_{21}^o = S_{31}^o = \frac{2}{3} & \text{at } f = f_o \quad (14b) \end{cases}$$

For the second passband fe:

$$\begin{cases} S_{11}^e = \frac{1}{3}, S_{21}^e = -S_{31}^e = \frac{2}{3} & \text{at } f = f_e \quad (14c) \\ S_{11}^o = -1, S_{21}^o = S_{31}^o = 0 & \text{at } f = f_e \quad (14d) \end{cases}$$

C. TRANSFORMATION OF SINGLE-ENDED S-PARAMETER TO MIX-MODE S-PARAMETER FOR THE BALUN FILTER AND POWER-DIVIDER

According to the port definition in Fig. 2, the mix-mode scattering matrix Smm for three-port dual-band balun filter can be determined as,

$$[S_{mm}] = \begin{bmatrix} S_{ss11} & S_{sd12} & S_{sc12} \\ S_{ds21} & S_{dd22} & S_{dc22} \\ S_{cs21} & S_{cd22} & S_{cc22} \end{bmatrix} \tag{15}$$

The relationship between its standard and mix-mode S-parameter is given as

$$[S_{mm}] = [M][S_{std}][M]^{-1} \tag{16}$$

where

$$[M] = \begin{bmatrix} 1 & 0 & 0 \\ 0 & \frac{\sqrt{2}}{2} & -\frac{\sqrt{2}}{2} \\ 0 & \frac{\sqrt{2}}{2} & \frac{\sqrt{2}}{2} \end{bmatrix} \tag{17}$$

For the five-port dual-band single to balanced power divider, the mix mode scattering matrix Smm can be determined as,

$$[S_{mm}] = \begin{bmatrix} S_{ss11} & S_{sc12} & S_{sc13} & S_{sd12} & S_{sd13} \\ S_{cs21} & S_{cc22} & S_{cc23} & S_{cd22} & S_{cd23} \\ S_{cs31} & S_{cc32} & S_{cc33} & S_{cd32} & S_{cd33} \\ S_{ds21} & S_{dc22} & S_{dc23} & S_{dd22} & S_{dd23} \\ S_{ds31} & S_{dc32} & S_{dc33} & S_{dd32} & S_{dd33} \end{bmatrix} \tag{18}$$

The relationship between its standard and mix-mode S-parameter is given as:

$$[S_{mm}] = [M][S_{std}][M]^{-1} \tag{19}$$

where

$$[M] = \begin{bmatrix} 1 & 0 & 0 & 0 & 0 \\ 0 & \frac{\sqrt{2}}{2} & \frac{\sqrt{2}}{2} & 0 & 0 \\ 0 & 0 & 0 & \frac{\sqrt{2}}{2} & \frac{\sqrt{2}}{2} \\ 0 & \frac{\sqrt{2}}{2} & -\frac{\sqrt{2}}{2} & 0 & 0 \\ 0 & 0 & 0 & \frac{\sqrt{2}}{2} & -\frac{\sqrt{2}}{2} \end{bmatrix} \tag{20}$$

REFERENCES

[1] L.-P. Feng and L. Zhu, "Compact wideband filtering balun using stacked composite resonators," *IEEE Access*, vol. 6, pp. 34651–34658, 2018.

[2] M. Du, K. Chen, J. Zhao, and Y. Feng, "Differential signal propagation in spoof plasmonic structure and its application in microwave filtering balun," *IEEE Access*, vol. 8, pp. 109009–109014, 2020.

[3] L.-P. Feng and L. Zhu, "Wideband filtering balun on a novel hybrid multimode resonator with the functionality of vertical transition," *IEEE Trans. Compon., Packag., Manuf. Technol.*, vol. 7, no. 8, pp. 1324–1330, Aug. 2017.

[4] J.-M. Yan, H.-Y. Zhou, and L.-Z. Cao, "A novel filtering balun and improvement of its isolation performance," *IEEE Microw. Wireless Compon. Lett.*, vol. 27, no. 12, pp. 1056–1058, Dec. 2017.

[5] S. Carpenter, M. Abbasi, and H. Zirath, "Fully integrated D-band direct carrier quadrature (I/Q) modulator and demodulator circuits in InP DHBT technology," *IEEE Trans. Microw. Theory Techn.*, vol. 63, no. 5, pp. 1666–1675, May 2015.

[6] Y. Peng, L. Zhang, J. Fu, and Y. Wang, "Analysis and design of a broadband SiGe HBT image-reject mixer integrating quadrature signal generator," *IEEE Trans. Microw. Theory Techn.*, vol. 64, no. 3, pp. 688–698, Mar. 2016.

[7] H. Wei, C. Meng, J. Su, S. Yu, and G. Huang, "17-GHz pHEMT Gilbert single-quadrature downconverter with polyphase filters for image rejection," in *Proc. Asia–Pacific Microw. Conf.*, Yokohama, Japan, Dec. 2010, pp. 690–693.

[8] S. Muralidharan, K. Wu, and M. Hella, "A compact low loss single-ended to two-way differential power divider/combiner," *IEEE Microw. Wireless Compon. Lett.*, vol. 25, no. 2, pp. 103–105, Feb. 2015.

[9] W. Zhang, Y. Liu, Y. Wu, and A. Hasan, "Novel planar compact coupled-line single-ended-to-balanced power divider," *IEEE Trans. Microw. Theory Techn.*, vol. 65, no. 8, pp. 2953–2963, Aug. 2017.

[10] H. Zhu, P. Qin, and Y. J. Guo, "Single-ended-to-balanced power divider with extended common-mode suppression and its application to differential 2×4 butler matrices," *IEEE Trans. Microw. Theory Techn.*, vol. 68, no. 4, pp. 1510–1519, Apr. 2020.

[11] W. Feng, Y. Zhao, W. Che, R. Gomez-Garcia, and Q. Xue, "Single-ended-to-balanced filtering power dividers with wideband common-mode suppression," *IEEE Trans. Microw. Theory Techn.*, vol. 66, no. 12, pp. 5531–5542, Dec. 2018.

[12] S. Li, X. Wang, J. Wang, and L. Ge, "Design of compact single-ended-to-balanced filtering power divider with wideband common-mode suppression," *Electron. Lett.*, vol. 55, no. 17, pp. 947–949, Aug. 2019.

[13] S.-W. Wong, F. Deng, Y.-M. Wu, J.-Y. Lin, L. Zhu, Q.-X. Chu, and Y. Yang, ''Individually frequency tunable dual- and triple-band filters in a single cavity,'' *IEEE Access*, vol. 5, pp. 11615–11625, 2017.
[14] J. Xu, K. Bi, X. Zhai, Y. Hao, and K. D. Mcdonald-Maier, "A dual-band microwave filter design for modern wireless communication systems," *IEEE Access*, vol. 7, pp. 98786–98791, 2019.
[15] D. Li, J.-A. Wang, Y. Liu, and Z. Chen, ''Miniaturized dual-band bandpass filter with sharp roll-off using ring-loaded resonator,'' *IEEE Access*, vol. 8, pp. 25588–25595, 2020.
[16] M.-H. Weng, S.-W. Lan, S.-J. Chang, and R.-Y. Yang, ''Design of dual-band bandpass filter with simultaneous narrow- and wide-bandwidth and a wide stopband,'' *IEEE Access*, vol. 7, pp. 147694–147703, 2019.
[17] X. Zhu, T. Yang, P.-L. Chi, and R. Xu, ''Novel reconfigurable single-to-balanced, power-dividing, and single-ended filter with frequency and bandwidth control,'' *IEEE Trans. Microw. Theory Techn.*, vol. 67, no. 2, pp. 670–682, Feb. 2019.
[18] X. Zhu, T. Yang, P.-L. Chi, and R. Xu, "A tunable single-to-balanced bandpass filter with bandwidth control," in *Proc. Asia–Pacific Microw. Conf. (APMC)*, Kyoto, Japan, Nov. 2018, pp. 1–3.
[19] P.-L. Chi and T. Yang, ''Novel 1.5-1.9 GHz tunable Single-to-Balanced bandpass filter with constant bandwidth,'' *IEEE Microw. Wireless Compon. Lett.*, vol. 26, no. 12, pp. 972–974, Dec. 2016.
[20] J. S. Hong and M. J. Lancaster, *Microstrip Filter for RF/Microwave Applications*. New York, NY, USA: Wiley, 2001.
[21] W. R. Eisenstadt, B. Stengel, and B. M. Thompson, *Microwave Differential Circuit Design Using Mixed-Mode S-Parameters*. Boston, MA, USA: Artech House, 2006.
[22] L. Gao and G. M. Rebeiz, "A 0.97–1.53-GHz tunable four-pole bandpass filter with four transmission zeroes," *IEEE Microw. Wireless Compon. Lett.*, vol. 29, no. 3, pp. 195–197, Mar. 2019, doi: 10.1109/LMWC.2019.2895558.
[23] L. Gao, T.-W. Lin, and G. M. Rebeiz, ''Design of tunable multi-pole multi-zero bandpass filters and diplexer with high selectivity and isolation,'' *IEEE Trans. Circuits Syst. I, Reg. Papers*, vol. 66, no. 10, pp. 3831–3842, Oct. 2019.
[24] J. Wang, F. Huang, L. Zhu, C. Cai, and W. Wu, ''Study of a new planar-type balun topology for application in the design of balun bandpass filters,'' *IEEE Trans. Microw. Theory Techn.*, vol. 64, no. 9, pp. 2824–2832, Sep. 2016.
[25] F. Huang, J. Wang, K. Aliqab, J. Hong, and W. Wu, "Analysis and design of a new self-packaged wideband balun bandpass filter with the functionality of impedance transformation," *IEEE Trans. Microw. Theory Techn.*, vol. 67, no. 6, pp. 2322–2330, Jun. 2019.
[26] G. M. Rebeiz, K. Entesari, and I. C. Reines, ''Tuning in to RF MEMS,'' *IEEE Microw. Mag.*, vol. 10, no. 5, pp. 55–71, Oct. 2009.

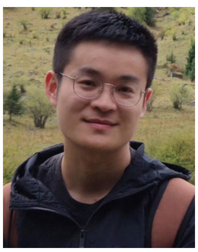

XIONG CHEN was born in Chengdu, Sichuan, China. He is currently pursuing the Ph.D. degree in electromagnetic field and microwave technology with the University of Electronic Science and Technology of China, Chengdu.

His current research interests include millimeter-wave circuit theory and technology, passive microwave, and millimeter-wave components.

TAO YANG (Senior Member, IEEE) received the B.Eng. and Ph.D. degrees from the University of Electronic Science and Technology of China (UESTC), Chengdu, China, in 2005 and 2011, respectively.

From September 2008 to September 2010, he was a Visiting Scholar with the Electrical Engineering Department, University of California at Los Angeles (UCLA). From August 2011 to September 2012, he was with the Institut d'Electronique et de Telecommunications de Rennes (IETR) and the Université de Rennes 1, Rennes, France. From October 2012 to April 2014, he was with the Department of Electrical and Computer Engineering, University of California at San Diego (UCSD). From April 2014 to February 2016, he was with Qualcomm Inc., San Diego, CA, USA. From February 2016 to September 2017, he was a Research and Development IC Engineer with Broadcom Ltd., San Jose, CA, USA. He is currently a Professor with UESTC. His research interests include Ka-band circuit designs, such as Ka-band frequency synthesizers and transceivers, miniaturized passive microwave and millimeter-wave components, such as filters, diplexers, triplexers, and baluns, broadband microstrip antennas and leaky-wave antennas, metamaterial-based microwave circuits, design and development of RF passive components for highly integrated RF integrated circuits in deep sub-micrometer CMOS and silicon-on-insulator (SOI) technologies, and development of high Q FBAR resonators and filters.

PEI-LING CHI (Senior Member, IEEE) received the B.S. and M.S. degrees in communication engineering from National Chiao Tung University (NCTU), Hsinchu, Taiwan, in 2004 and 2006, respectively, and the Ph.D. degree in electrical engineering from the University of California at Los Angeles (UCLA), in 2011.

Since 2011, she has been an Assistant Professor of electrical and computer engineering with National Chiao Tung University, where she is currently an Associate Professor. She holds several U.S. and international patents in the area of the left-handed metamaterials. Her research interests include the analysis and design of the left-handed metamaterial circuits, design of microwave components and integrated systems, and development of millimeter-wave/terahertz antennas and communications.

Dr. Chi was a recipient of the Research Creativity Award from the National Science Council, Taiwan, in 2004.